Concurrent Binding to Multiple Ligands: Kinetic Rates of CD16b for Membrane-Bound IgG1 and IgG2

Tom E. Williams,* Periasamy Selvaraj,† and Cheng Zhu*

*George W. Woodruff School of Mechanical Engineering and Georgia Tech/Emory Department of Biomedical Engineering, Georgia Institute of Technology, Atlanta, Georgia 30332-0363 and †Department of Pathology and Laboratory Medicine, Emory University School of Medicine, Atlanta, Georgia, 30322 USA

ABSTRACT CD16b (FcγRIIIb) is the most common receptor for the Fc domain of IgG on leukocytes. The binding of Fc receptors to immunoglobulin triggers a wide array of immune responses. In published assays measuring the reaction of CD16b with isotypes of soluble IgG, the affinity for IgG1 was low and that for IgG2 was undetectable. Here we report the first measurement of kinetic rates of CD16b binding to membrane-bound IgG isotypes—a physically distinct and physiologically more relevant presentation—using a recently developed micropipette method. In contrast to the soluble data, we found clearly measurable IgG2 binding, with a forward kinetic rate six-fold lower than that of IgG1 but with an equilibrium affinity only threefold lower. This suggests a nonnegligible role for IgG2 in Fc-mediated immune responses, particularly in longer duration contacts. The binding constants were measured from two sets of experiments. Single-isotype experiments were analyzed by an existing model (Chesla et al., 1998, *Biophys. J.* 75:1553–1572). The resulting kinetic rates were used as input to an extended model (Zhu and Williams, 2000, *Biophys. J.* 79:1850–1857.) to predict the results of mixed-isotype experiments. This design enabled rigorous validation of the concurrent binding model through a test of its predictive ability.

INTRODUCTION

Immunoglobulins (Ig), or antibodies, are central components of the immune system. Of the five classes of human antibodies, IgG is by far the most common, making up about 80% of all antibodies in normal adult serum. IgG is produced in four subclasses, or isotypes. IgG1, with a typical concentration of ~6–9 mg/ml in plasma, makes up about 60% of total IgG. IgG2 is normally present in serum at ~3–4 mg/ml or about 30% of total IgG. In contrast to these dominant isotypes, IgG3 and IgG4 comprise, respectively, only 6% and 3% of total IgG (Fridman, 1997).

Circulating IgG binds to foreign particles or damaged tissue by direct recognition through dual, highly variable, antigen binding fragments (Fab). The highly conserved Fc fragment of this bifunctional molecule is available for binding by Fcγ receptors (FcγRs) on the cell surface. Such an interaction may trigger a cascade of effector functions that may include cytokine release, immune complex clearance, receptor-mediated phagocytosis, antibody-dependent cellular cytotoxicity, and enhancement of antigen presentation (Selvaraj et al., 1989; Salmon et al., 1996; Rascu et al., 1997; Clynes et al., 1998; Lowry et al., 1998). For this reason, it is of great interest to characterize the IgG–FcγR interactions. Although it has been noted for some time that the immune system responds to different pathogens with a specific mix of IgG isotypes, very little is known about the nature of their individual roles. With the exception of the $Fc\gamma RIIa^{H131}$ allotype which binds IgG2 well (Warmerdam et al., 1990; Clark et al., 1991; Rascu et al., 1997), affinity measurements for soluble ligands have shown that FcγRs interact with human IgG1 and IgG3 much more readily than with IgG2 or IgG4 (Huizinga et al., 1989; Powell et al., 1996; Fridman, 1997; Rascu et al., 1997). In fact, in most cases, any association between FcγRs and these latter isotypes was undetectable by the methods used. Nevertheless, a clear correlation is seen between low IgG2 levels and respiratory tract infections (Jefferis and Kumararatne, 1990).

Clues to the varied affinities of FcγRs for each isotype are seen in the quaternary structure of IgG. The most striking structural differences between the isotypes lie in the hinge region connecting Fab fragments with the Fc fragment (Fig. 1). The hinge region of IgG1 includes two disulfide bridges near the first Fc globular domains (Cγ2). Critical epitopes for FcγR binding to all IgG isotypes appear on Cγ2 (Burton, 1985). Rotational diffusion assays have indicated that the IgG1 Fab fragments can flap as well as rotate about their axes. This may give it an advantage in both binding an antigen and providing FcγRs access to the critical Cγ2 epitopes. IgG2 has a hinge region of similar dimension as IgG1, but has two additional disulfide bridges located near the base of the Fab fragments. This is likely to greatly reduce flapping and may completely prevent axial rotation of the Fab fragments.

The Fcγ receptors are a widely displayed family of cell surface glycoproteins with varying affinity for the Fc fragment of γ-chain-expressing Ig (IgG) (Fridman, 1989; Powell et al., 1996; Sautes, 1997). Of the three classes of FcγRs (FcγRI, FcγRII, and FcγRIII or CD64, CD32, and CD16, respectively) and various isoforms within each class (e.g.,

Received for publication 27 September 1999 and in final form 6 July 2000.

Address reprint requests to Cheng Zhu, George W. Woodruff School of Mechanical Engineering and Georgia Tech/Emory Department of Biomedical Engineering, Georgia Institute of Technology, Atlanta, Georgia 30332-0363. Tel.: 404-894-3269; Fax: 404-385-1397; E-mail: cheng.zhu@me.gatech.edu.

0006-3495/00/10/1858/09 $2.00

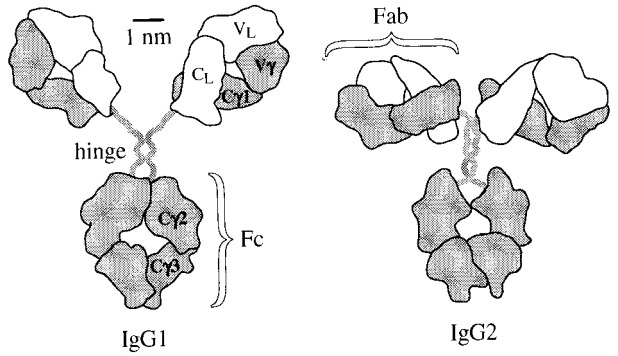

FIGURE 1 Structure of the human IgG isotypes 1 and 2. Isotypes of IgG differ noticeably in the structure of their hinge regions, which connect the two variable antigen-binding Fab fragments to the conserved effector-stimulating Fc fragment. Additional disulfide bonds in the IgG2 hinge may limit access to the Cγ2 regions, which contain critical epitopes for Fc receptor binding.

CD16a and CD16b), FcγRIIIb (CD16b) is unique in four aspects: It is the predominant Fc receptor in blood; it is exclusively expressed on granulocytes; it anchors to the cell membrane by means of a glycosyl phosphatidylinositol (GPI) moiety without transmembrane and cytoplasmic domains; and it has no associated side chains (Selvaraj et al., 1988; Sautes, 1997). Although a number of groups have measured the affinity of Fc receptors to soluble Ig (Fridman, 1989; Huizinga et al., 1989; Powell et al., 1996; Rascu et al., 1997), there have been no published reports outside of our lab regarding the fundamentally different—and physiologically more relevant—characteristics of binding to surface-bound ligand. In our previous work (Chesla et al., 1998), a micropipette method was developed and used to measure the two-dimensional (2D) kinetics of CD16a binding to total serum IgG. In addition to the distinct membrane anchor, CD16b differs from CD16a by six amino acids in the extracellular domain. CD16b also possesses an even lower affinity for soluble IgG than does CD16a (Chesla et al., 2000). The major objective of this work was to use the micropipette method to characterize the 2D kinetic rates and equilibrium affinity of CD16b for the two most common human IgG isotypes, IgG1 and IgG2, and to compare this with the receptor's interaction with soluble IgG.

To satisfy a parallel objective, the experiments were designed so that the data gathered could be used to rigorously test the validity of a new model for concurrent binding of multiple species of receptors and ligands. This scenario more closely approximates the in vivo situation, where cell adhesion frequently involves simultaneous interactions of several species of receptors and ligands. As such, the overall adhesive outcome cannot be definitively attributed to any particular species and may even involve bonds of multiple species. However, given a large number of similar opportunities for adhesion, the concurrent binding model can be used to probabilistically relate the observed adhesion frequency to the average numbers of bonds of all species, expressed in terms of their respective kinetic rates. The model described in the previous companion paper (Zhu and Williams, 2000) is completely general in the specification of the receptor and ligand populations; that is, any number of different receptors and ligands may be present. In this paper and the next (Williams et al., 2000), two special cases are examined for the dual purposes of validating the model and gathering useful information on the kinetics of Fc receptor binding. In this paper, data is presented from experiments in which a single receptor, CD16b, was present and two isotypes of IgG, IgG1 and IgG2, were treated as distinct ligands.

MATERIALS AND METHODS

Antibodies and cells

For radioimmunoassay (RIA), murine monoclonal antibody (mAb) CLB-Fcgran1 (anti-CD16) was purified from hybridoma supernatant by protein G affinity chromatography, cleaved into Fab fragments by Lampire (Pipersville, PA), and iodinated in Iodogen-coated Eppendorf tubes. For flow cytometry, supernatant of hybridoma-secreting CLBFcgran1 was used at saturating dilutions without purification. GG7 (anti-human Fcγ mAb) was obtained as ascites fluid from Sigma Chemical Company (St. Louis, MO). FITC-conjugated polyclonal goat anti-mouse IgG (Sigma) was used as the secondary antibody.

Lyophilized human IgG1 and IgG2 from myeloma plasma were obtained from Sigma. After resuspension in unbuffered saline (1 mg/ml), aliquots were stored at 4°C. Erythrocytes were isolated from whole blood of normal healthy volunteers according to the following procedure. Approximately 7 ml whole blood was collected by venipuncture into sterile Vacutainers (Becton Dickinson, San Jose, CA) containing EDTA. This was carefully layered over 3 ml of Histopaque 1119 and centrifuged (30 min, 700 $\times$ *g*, room temperature). The supernatant was removed and the pelleted erythrocytes washed once in red blood cell (RBC) storage solution (EAS45) (Dumaswala et al., 1996). RBCs were stored aseptically at 4°C in EAS45/penicillin/streptomycin, at ~20% hematocrit for up to three weeks with negligible hemolysis.

Chinese hamster ovary cells (CHO-K1) transfected to express CD16b (NA2 allotype), and nontransfected CHO-K1 cells, have been described (Nagarajan et al., 1995). CHO cells were cultured in RPMI 1640 media plus 10% fetal calf serum according to standard practices. Transfectant CHO cell media were supplemented with 400 μg/ml hygromycin as the selection agent. CLBFcgran1 hybridoma cultures were weaned to 2% fetal calf serum in OptiMEM (Gibco BRL, Grand Island, NY) or 5% Ultra-low IgG FBS (Gibco) in RPMI prior to collection of supernatant. RPMI media was supplemented with an additional 2 g/l glucose and 2 mM GlutaMax (Gibco) (Nayve et al., 1994). Large-scale production of supernatant was performed in sealed 2-liter roller bottles, and occasionally in large-capacity T-flasks. When sealed bottles were used, the media was supplemented with 5 mM HEPES buffer (Reuveny et al., 1986). Initial cell density was chosen based on the growth rate such that maximum densities would be reached in six days or less.

Chromium chloride coupling of IgG to RBCs

Human IgG was covalently coupled to the membranes of RBCs by means of a chromium chloride ($CrCl_3$) method previously described (Chesla et al., 1998). For mixed-isotype preparations, saline solutions of IgG1 and IgG2 (1 mg/ml) were combined in the desired ratio (2:1 or 1:2) prior to coupling. Cells were subsequently washed and stored in EAS45. Aliquots (1 μl) from

each coupled sample were examined under light microscopy for excessive aggregation. Samples were assayed for coating density and sample uniformity by flow cytometry. In this assay the optimal ratios of protein to $CrCl_3$ were determined empirically following a grid design. Although increasing levels of $CrCl_3$ consistently increased the coating levels, this also increased the degree of cell aggregation. Increasing amounts of protein decreased aggregation, but did not necessarily increase the coating densities. In fact, excessive amounts of protein quenched the $CrCl_3$ reaction completely.

This coupling method can provide very high coating densities and involves a nonspecific reaction between the carboxyl groups on the soluble protein and the RBC membrane proteins. It therefore is likely to result in a spatially uniform and randomly oriented presentation of the bound IgG. Coated RBCs remain quite flexible under micropipette manipulation and are structurally similar to untreated RBCs upon examination by scanning electron microscopy (Williams, 1998).

Site density determination

Site densities of IgG on RBCs were determined by quantitative indirect fluorescent immunoassay (QIFI) (Poncelet and Carayon, 1985; Bikoue et al., 1996; Serke et al., 1998) using an LFA-3 site density of 3900 molecules/RBC as the reference standard (Selvaraj et al., 1987). Samples were prepared for flow cytometry using the usual two-step staining protocol. IgG-coated RBCs were incubated with anti-human Fcγ (GG7, 1:1000 ascites fluid), anti-LFA-3 (TS2/9 culture supernatant), or isotype-matched negative control mAb (X63 culture supernatant) as first-step antibodies. GG7 is highly reactive with all human IgG subclasses, and so total IgG density was obtained. An Fc-specific FITC-conjugated goat anti-mouse IgG (same lot) was used as the second-step reagent for all samples. The median fluorescence (corrected for X63 nonspecific binding) relative to LFA-3 was used to estimate site density of IgG.

The CD16b expression on the CHO cell transfectants was observed by flow cytometry to be stable under the culture conditions described earlier. Receptor site density was quantified by RIA using ^{125}I-labeled anti-CD16 mAb. ^{125}I-Fab CLBFcgran1 was incubated with cells at a saturating concentration (2.4 μg/ml). Triplicate samples were thoroughly washed and counted, with the cell-bound radioactivity measured on a gamma counter. Nontransfected cells were used as negative controls. Readings were converted to site densities using specific activity of the ^{125}I-mAb, determined in parallel from standard samples (2 μl aliquots of ^{125}I-Fab). The mean expression level was 9.3×10^5 per cell, or about 1600/μm^2, based on an apparent surface area of 580 μm^2. With IgG coatings of 800–1000/μm^2, this provided an excess of receptors and ligands relative to the anticipated number of bonds, ensuring that the effects of competition would be negligible (Zhu and Williams, 2000).

For the purposes of the analysis in this work, it was assumed that receptors and ligands that were accessible by the antibodies described, and therefore quantifiable by QIFI or RIA, were also available to each other in the micropipette binding-frequency assay. An availability factor of less than one would lead to an underestimation of A_cK_a and A_ck_f by this factor, but would not affect the central comparative results presented in this paper (Chesla et al., 1998).

Micropipette binding-frequency assay

The micropipette system and the binding-frequency assay have been described in detail previously (Chesla et al., 1998). Briefly, narrow glass pipettes (2–3 μm inner diameter for RBCs, 5–8 μm i.d. for CHO cells) were prepared using a micropipette puller (Kopf, Tujunga, CA). Used RBC pipettes were frequently stored for several weeks in capped RIA tubes containing acetic acid, diluted 1:30 in de-ionized distilled H_2O. Before use, the storage solution was removed by displacement with a large-gauge needle and backfilled with chamber solution by means of high suction. Chamber solution was Hank's Balanced Salt Solution with phenol red and without calcium or magnesium, diluted to 45–55% with de-ionized distilled H_2O, supplemented with 1% IgG-free BSA (Sigma) and sterile filtered just prior to use. Chambers were mounted on a Zeiss inverted microscope (Axiovert 100, Oberkochan, Germany) with an attached CCD camera. Following introduction of cells to the chamber, one CHO cell and one RBC were gently aspirated and aligned with a small axial gap between them. Selected CHO cells were healthy and of a consistent, roughly average, size. The RBC pipette was connected to a computer-controlled piezoelectric actuator that was programmed to move its cell a fixed distance at a uniform rate of 10 μm/s. Cells remained in contact, allowing zero-force kinetics to proceed for a prescribed duration, and then retracted. An adhesion, indicating the presence of at least one bond at the moment of retraction, was confirmed by the deflection of the RBC membrane. One hundred contact cycles were conducted for each cell pair with multiple cell pairs tested at each contact duration. Contact durations ranged from 1 to 16 s, which covered both the transient phase and the steady-state binding of the interaction in question. Data in such a range are required to get good estimates for both kinetic rates and equilibrium binding affinity. Adhesion frequency was used as an estimate for the probability of an adhesion to be present at the end of the contact time under the condition being tested. Background-subtracted images were viewed in real time on a monitor and stored on videotape for future analysis. In initial studies with this receptor–ligand system, RBC aspiration pressures were tested over a range of 2–8 mm H_2O (effectively tuning the RBC to different force-detection thresholds) with no change in adhesion frequency, confirming that the measurement accuracy was not limited by the ability to detect the weakest interactions. The threshold of detection was below 2 pN, ensuring that essentially no specific bonds would go undetected. At the other extreme of forces, very strong bonds could lead to extraction of the proteins from the membrane. However, the typical running frequency of adhesion was stable over a hundred cycles, indicating that, if extraction of receptor or ligand occurred at all, the surface densities of unbound protein were sufficiently high to negate any impact on the binding kinetics.

Data analysis

Equilibrium affinity and kinetic rates were extracted from the binding frequency data by iteratively reweighted nonlinear regression to the single-species model (Chesla et al., 1998) or the concurrent binding model (Zhu and Williams, 2000) using the Levenberg–Marquardt algorithm (Wolfram Research, 1996). After analysis of the single-isotype data, prediction intervals (with 95% confidence levels) were computed for the expected mean response of the mixed-isotype experiments, assuming the validity of the concurrent binding model. Details of the weighting method and the prediction interval calculation are presented in the Appendix.

RESULTS

Binding to RBCs coated with single IgG isotypes

As shown in Fig. 2, for the interaction of the CD16b-transfected CHO cells with RBCs coated with human IgG1, a ligand coating density of 1000 IgG1/μm^2 resulted in a binding frequency of about 50% at equilibrium. However, RBCs coated with a similar density of IgG2 exhibited equilibrium binding of only 22%. It is also apparent that the binding of CD16b with IgG1 reached equilibrium faster than with IgG2. Adhesions mediated by both IgG isotypes were well above the 5% nonspecific binding of the same CD16b-transfected CHO cells to RBCs coated with IgG-free ovalbumin by means of the same chromium chloride coupling procedure. Binding specificity for our CD16-ex-

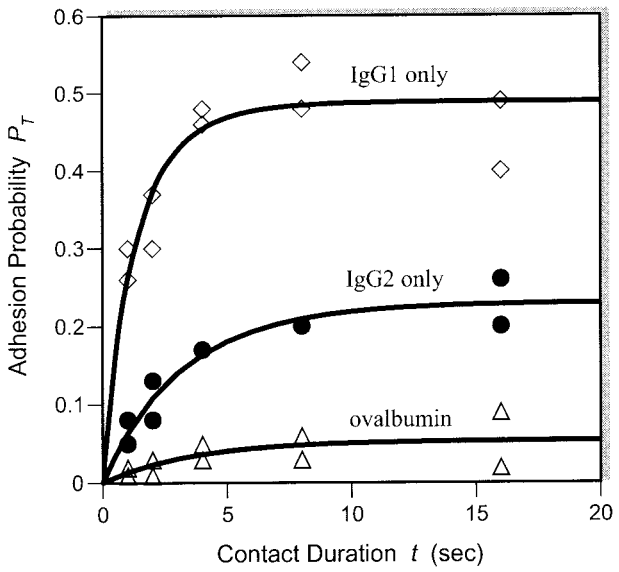

FIGURE 2 Single-isotype binding curves. CD16b-expressing CHO cells were held in contact with RBCs coated with human IgG1 (◇) at 1000 molecules/μm^2, IgG2 (●) at 980 molecules/μm^2, or IgG-free ovalbumin (△). Each point represents total adhesion probability estimated from one cell pair with 100 cycles of contact. IgG curves were calculated according to $P_T = P_N + P_S - P_N P_S$, where P_N and P_S are given by Eqs. 1 and 2, respectively, based on the best-fit parameters (Zhu and Williams, 2000).

pressing CHO cell/IgG-coated RBC system has been shown previously by extensive control experiments (Chesla et al., 1998, 2000; Williams et al., 2000).

Prior to analysis of the specific binding data, a smooth curve was fit through the nonspecific data according to the form

$$P_N = 1 - \exp[-a(1 - e^{-bt})]. \quad (1)$$

This function has two free parameters, rises from 0 at $t = 0$ and asymptotically approaches an equilibrium level of $1 - e^{-a}$ as $t \to \infty$. This is identical to the structure of the specific binding (compare with Eq. 2 below), though here we have made no efforts toward physical interpretation of the parameters a (= 0.05) and b (= 0.3 s^{-1}). The quality of the fit to the ovalbumin data in Fig. 2 supports the use of this function.

Analysis of the single isotype data proceeded by removing the smoothed nonspecific component estimated from Eq. 1 from each observed total binding probability; that is, $P_S = (P_T - P_N)/(1 - P_N)$ where subscripts denote specific, nonspecific, and total adhesions, assuming specific and nonspecific binding to be independent rather than mutually exclusive events (Zhu and Williams, 2000). Fitting the resulting data, along with the known predictor variables (receptor and ligand surface densities m_r and m_ℓ, contact duration t) to the single-species binding model (Chesla et al., 1998),

$$P_S = 1 - \exp\{-m_r m_\ell A_c K_a [1 - \exp(-k_r t)]\}, \quad (2)$$

yielded estimates for the regression parameters $A_c K_a$ (the 2D binding affinity scaled by the constant but unknown contact area A_c) and k_r (the reverse rate constant). The forward 2D rate constant (scaled by A_c) $A_c k_f$ was calculated from the relationship $K_a = k_f/k_r$. The IgG1-only and the IgG2-only data were separately regressed to this model and the derived estimates for the binding constants and their standard errors are listed in Table 1. The solid lines shown on Fig. 2 represent the associated best-fit curves. It is evident that the agreement between the data and the fitted curves is quite good, providing further support for the single-species kinetic model of Chesla et al. (1998).

Prediction intervals for the mean mixed-isotype response

Using the data obtained from the single-isotype experiments, we wanted to make predictions about the adhesion probability for mixed-isotype experiments, based on the concurrent binding model. Following the methods described in the Appendix, prediction intervals (with 95% confidence levels) for the mean response under concurrent binding were calculated. The calculation used, as input, two sets of binding affinities and reverse rates (and their associated covariance matrix) determined from the single-isotype experiments and ligand densities m_{ℓ_1} (for IgG1) and m_{ℓ_2} (for IgG2) matching those of the mixed-isotype experiments. The two prediction intervals are shown in Fig. 3 (*paired curves*).

It should be noted that prediction intervals for the mean response provide insight into the distribution of the expected means, not the distribution of the expected data, which is generally much broader. Mean response prediction intervals continually narrow as the amount of incorporated data increases, whereas prediction intervals for the data distribution approach a finite spread reflecting the characteristic variation of the system elements. Because of this dependence on the data set size, the prediction intervals generated from the single-isotype data were compared to mean responses obtained from a similar quantity of dual-isotype data.

TABLE 1 Summary of binding parameters for CD16b^{NA2}

	$A_c K_a$ (10^{-7} μm^4)		k_r (s^{-1})	
Ligand Coating	IgG1	IgG2	IgG1	IgG2
IgG1 only	3.8 ± 0.2	—	0.64 ± 0.11	—
IgG2 only	—	1.3 ± 0.2	—	0.29 ± 0.10
Mixed isotypes only	4.4 ± 0.4	1.6 ± 0.5	0.84 ± 0.20	0.10 ± 0.21
All data	4.0 ± 0.2	1.4 ± 0.2	0.70 ± 0.11	0.28 ± 0.10

n = 10, 8, 20, and 38 cell pairs (100 contact cycles each), respectively, for each ligand-coating set above. An additional 10 cell pairs were used to characterize the nonspecific binding.
Values are mean ± SE.

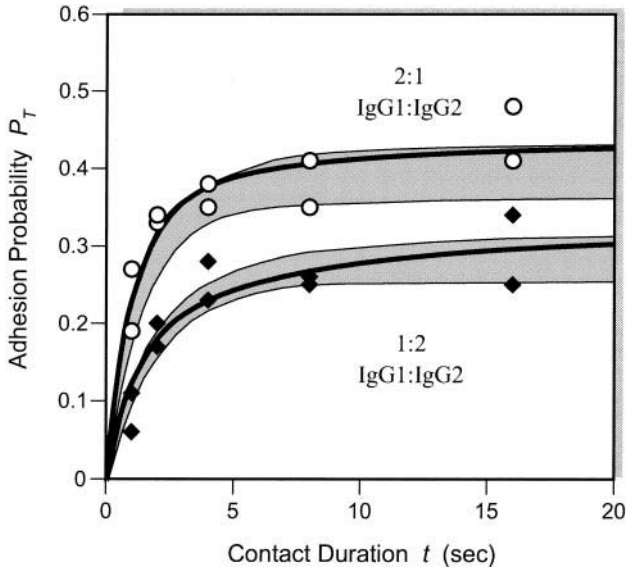

FIGURE 3 Dual-isotype binding curves. CD16b-expressing CHO cells were held in contact with RBCs coated with ratios of IgG1:IgG2 of 2:1 (○) or 1:2 (◆). Total IgG content was 890 and 780 molecules/μm^2, respectively. Solid curves represent the weighted least-squares fits of all dual-species data to the concurrent binding model. Gray regions represent the 95% prediction intervals for the means obtained from inserting the single-species results into the concurrent binding model. Nonspecific binding was included in these P_T curves in the same manner as the single-isotype analysis (cf. Fig. 2 legend). Each point represents one cell pair with 100 cycles of contact.

Binding to RBCs coated with mixed IgG isotypes

Mixed-isotype coatings were prepared with a ratio of IgG1 to IgG2 of either 2:1 or 1:2. As shown in Fig. 3, both samples displayed binding time courses between the two single-isotype data (Fig. 2), with the binding of the 2:1 ratio sample somewhat more frequent than that of the 1:2 ratio sample. For comparable total densities of IgG, this sequential laddering of the data from low to high as IgG1 content increases and IgG2 content decreases is consistent with an equilibrium binding affinity of CD16b for IgG1 substantially higher than that for IgG2, as suggested by the soluble binding assays. It was an important consideration in our experimental design to use two IgG isotypes with substantially different kinetic rates and binding affinities to CD16b. Similar binding constants for the two ligand species would have led to similar time courses for the adhesion probability regardless of the mixing ratios. Although the assay would have still yielded kinetic data, it would not have provided an adequately rigorous test of the concurrent binding model, because this model would have collapsed to the single-species form, leaving the multi-species extension completely unexplored.

The two sets of mixed-isotype data in Fig. 3 were fit simultaneously to the concurrent binding model (Zhu and Williams, 2000),

$$P_S = 1 - \exp(-\langle n_1\rangle - \langle n_2\rangle)\,, \tag{3a}$$

where

$$\langle n_i\rangle = m_r m_{\ell_i} A_c K_{ai}[1 - \exp(-k_{ri}t)] \tag{3b}$$

may be interpreted as the average number of bonds per contact that is mediated by the ith IgG isotype. The specific binding probability data were determined by removal of the smoothed nonspecific data from the total binding observed, as was done in the single-isotype analysis discussed above. Use of the multispecies version of the concurrent binding model involves the simultaneous determination of affinity and reverse rate constants for all ligands present, IgG1 and IgG2 in this case. The values and standard errors for the four binding constants obtained in this manner are listed in Table 1. The best-fit curves associated with these parameters (Fig. 3) represent estimates of the mean behavior for the mixed-isotype binding conditions. The best-fit concurrent binding curves generated from the dual-isotype data fall within the prediction intervals generated from the single-isotype data at virtually all times.

Best estimates for the binding constants

The kinetic rate and binding affinity constants describing the interaction of CD16b and the human IgG isotypes 1 and 2 were independently estimated from the single-species data and the dual-species data. The ability for the binding constants derived from the single-species data to successfully predict the mixed IgG isotype experiments (Fig. 3) suggests that their values agree with the corresponding parameters estimated from the dual-species data. This is indeed the case (Table 1). Through the use of the concurrent binding model, it was also possible to incorporate the entire data set (48 cell pairs, including 10 lacking IgG) into a single best estimate of these parameters. Results from this analysis are also listed in Table 1.

DISCUSSION

A new sensitivity level demonstrated for the micropipette method

A major goal of the present work was to measure the 2D kinetic rate and binding affinity constants of the low affinity Fcγ receptor CD16b for the two most abundant IgG subtypes. In previous publications, the three-dimensional (3D) affinity of CD16b for soluble IgG2 has been stated as being extremely low (Powell et al., 1996) or nonexistent (Huizinga et al., 1989; Sautes, 1997). Therefore, it was expected to represent a challenge to our recently developed micropipette method. However, with sufficiently high densities of receptor and ligand, we were able to quantify both the affinity and kinetic rates with good resolution. Still, the

weakness of this interaction is illustrated by the fact that, even with the highest protein densities examined (1600 CD16b and 980 IgG2 per μm^2 in the IgG2-only case), specific adhesions were present at the end of only about 20% of the long-duration contacts (Fig. 2). The sensitivity of the 2D binding-frequency assay was demonstrated at a new level. The 2D equilibrium affinity of this receptor–ligand pair ($A_cK_a = 1.4 \times 10^{-7}$ μm^4) is the lowest of any previously reported affinities (Chesla et al., 1998, 2000).

The average number of bonds per adhesion can be calculated by dividing the average number of bonds per contact, $\langle n \rangle$, by the probability of specific adhesion, P_S. From Eq. 2, we see that this number was only about 1.1 for the above CD16b–IgG2 interaction. A caveat to the above calculation is that the micropipette-aspirated RBC adhesion detector must be sufficiently sensitive to ensure that no specific bonds would go undetected. This was investigated experimentally by measuring the dependence (or the lack thereof) of the detectable adhesion frequency on the RBC aspiration pressure. The tested range was 2–8 mm H_2O, corresponding to force detection thresholds from <2 pN to >10 pN. No changes in the measured adhesion frequency were found, confirming that the measurement accuracy was not limited by the sensitivity cutoff.

Validation of the concurrent binding model

A parallel goal of this paper was to test the model of concurrent binding of multiple molecular species developed in the companion paper (Zhu and Williams, 2000). A frequently used (although weak) test for the validity of a model is how well it fits experimental data. Here, a more challenging test was also devised, namely, how accurate the model predicts results from new experiments, using a priori knowledge obtained independently. Our approach was to divide the data into two groups—one that could be analyzed using an existing model and the other that would require the use of the extended model. Applying the existing single-species model to the first data group, kinetic rates were obtained describing how CD16b interacted with two human IgG isotypes individually when each was presented as a homogeneous population (Fig. 2). Next, this information was used as input to the extended dual-species model to *predict* how the receptor might interact simultaneously with the two ligands when both were presented as heterogeneous populations. The prediction was then compared to the actual data in the second group obtained from experiments with dual-isotypes mixed at two different ratios (Fig. 3). The excellent correspondence found in this comparison has thus provided substantial support for the probabilistic kinetics arguments upon which both the original single-species model and the new multi-species model rely.

Estimating the binding characteristics of CD16b to total serum IgG

In this study, the two predominant isotypes of human IgG have been treated as unique ligands. The substantial difference in their associated binding constants warrants this treatment. What then does this mean for interpretation of published FcγR kinetics experiments in which total human serum IgG is treated as a single ligand? In these cases, the binding constants determined are for an imaginary homogenized ligand, bearing characteristics that are a blend of those of the individual isotypes actually present (Zhu and Williams, 2000). In this work, for example, if we study the cells prepared from a 2:1 ratio of IgG1:IgG2 as if they expressed a single homogeneous ligand, then analysis of the data (using the single-species rather than the concurrent model) gives an affinity of 3.3×10^{-7} μm^4 and a reverse kinetic rate of 0.56 s^{-1}. Comparison with the values for the individual component isotypes in Table 1 illustrates the effects of homogenization. We also note that the 2:1 sample reasonably approximates total serum IgG, and so the values above represent an estimate for the binding parameters expected from similar experiments using total serum IgG-coated RBCs with the CD16b-expressing CHO cells.

Binding to membrane-bound ligands differs substantially from binding to the soluble forms

Although the affinity of CD16 for IgG has been measured in solution in some cases, for CD16-expressing leukocytes, it is affinity to immobilized antibody, bound to pathogens or damaged tissue, that is critical. This study represents the first measurements of CD16b affinities for immobilized IgG1 and IgG2. Our results show that the 2D equilibrium affinity of CD16b for IgG1 is about three times that for IgG2. Although this is a significant shortcoming, it should not prevent IgG2, immobilized to surfaces and in sufficient density, from participating in the stimulation of effector responses in CD16b-expressing neutrophils. The difference in the forward kinetic rate, however, is more dramatic. The reverse rate of IgG1 is about twice that of IgG2, so, from $K_a = k_f/k_r$, it is apparent that the forward rate of IgG1 must be about six times that of IgG2. The ability to form adhesions during very brief contacts in circulation ought to be a critical skill for cells of the immune system, in particular Fc receptor-bearing cells. From its low forward rate constant, it is apparent that IgG2 does a poor job of initiating such adhesions, but its low reverse rate suggests that it retains bonds longer than IgG1. This may indicate a more significant role for IgG2 in longer duration adhesions (>5 s) than in transient contacts. Figure 4 illustrates how the IgG2 to IgG1 bond ratio grows from less than 15% at the beginning of the contact to more than a third in equilibrium given equal densities of membrane-bound IgG1 and IgG2.

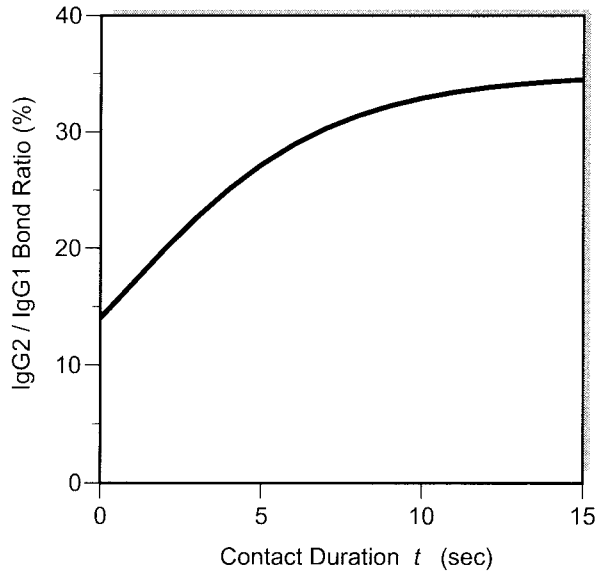

FIGURE 4 Relative participation of IgG2 in bond formation. When a CD16b-expressing cell encounters a surface with equal amounts of immobilized IgG1 and IgG2, almost all bond formation in the initial seconds of contact are mediated by IgG1. However, if contacts are maintained beyond five seconds, the relative participation of IgG2 will double due to its slower reverse rate.

It is surprising that the seemingly large relative 3D affinity of CD16b for IgG1 and IgG2 (IgG2 $K_a^{3D} \approx 0$) only translates into a mere threefold difference in 2D affinity. However, this is not an isolated case. The 2D affinity for total human IgG of CD16b^{NA2} (estimated in the preceding section using 2:1 IgG1:IgG2 data) is, respectively, about a half and a sixth of those of CD16a and CD16a-GPI, a chimeric molecule created by replacing the polypeptide transmembrane anchor of CD16a with the GPI anchor of CD16b (Chesla et al., 2000). By comparison, the 3D affinity of CD16b^{NA2}, measured by competitive inhibition using soluble total human IgG, is about a tenth and a hundredth of those of CD16a and CD16a-GPI, respectively (Chesla et al., 2000). This tremendous compression of the relative affinities in the 2D case demonstrates the distinctly different character of adhesion between membrane-bound molecules and the 3D soluble case. The underlying cause of this compression is a matter of current research and will require an understanding of both the protein conformation and its presentation by the membrane. This represents a challenge to the existing theory of 3D-to-2D affinity conversion (Bell, 1978; Bell et al., 1984; Kuo and Lauffenburger, 1993; Lauffenburger and Linderman, 1993; Dustin et al., 1996); and it emphasizes the need to measure 2D binding parameters directly.

APPENDIX

Most of the results of this paper are derived from nonlinear regression analysis of micropipette data. For completeness, the specific details of the approach used in this work are presented below.

Iteratively reweighted least-squares method

The weighted least-squares problem for model $y = f(\mathbf{x}, \mathbf{b})$ is to determine the fit parameters $\mathbf{b}$ by minimizing the weighted squared residuals ε^2 from N sets of observed responses y and predictor variables $\mathbf{x}$:

$$\min_{\mathbf{b}} \sum_{j=1}^{N} w_j \varepsilon_j^2 = \min_{\mathbf{b}} \sum_{j=1}^{N} w_j [y_j - f(\mathbf{x}_j, \mathbf{b})]^2 . \qquad \text{(A1)}$$

For the concurrent binding model (Eq. 3), the specific adhesion frequency P_S is the observed response (P_T may be used if specific and nonspecific binding are being regressed simultaneously), surface protein densities and contact time are the predictor variables, and affinities and reverse rates are the fit parameters. The N weights w_j are chosen to minimize heteroscedasticity. (The $w_j \equiv 1$ case is ordinary least-squares.)

Ordinary least-squares regression assumes that residuals are normally distributed about the best fit and that the variances of their distributions are equal for all the conditions examined. Heterogeneity of variance, or heteroscedasticity, will result in an inappropriate best fit and an inaccurate estimate of the standard errors of the regression parameters (Carroll and Ruppert, 1988). Figure 5 shows residuals from micropipette binding frequency experiments, illustrating the dependence of the variance of P on the response P. (Correlation between σ_P^2 and all predictor variables is also present, but not shown.) A weighting function was used to reduce the excessive heteroscedasticity in the data.

Choice of weighting function

The weights were chosen to be proportional to the inverse variances; that is, $w_j = c/\sigma_j^2$. The constant c has no effect on the fit, as can readily be seen from Eq. A1. The true variances σ_j^2 of the residual distributions are unknown and estimates of their relative magnitudes must be made. We chose to use several physical assumptions (described below) to develop a function for σ_P^2, and required that it display heteroscedasticity consistent with the residual data in Fig. 5.

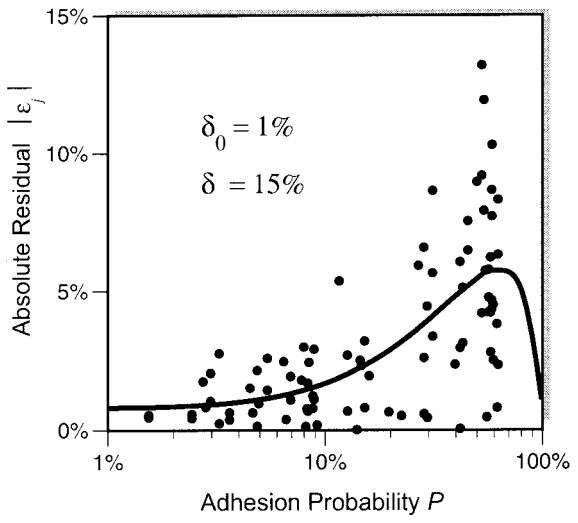

FIGURE 5 Dependence of residuals on adhesion probability P. The absolute values of the residuals following regression of the micropipette data shows considerable heteroscedasticity. The final weighting function (square root of Eq. A2) is shown, determined from the indicated best estimates for the free parameters δ_o and δ. The expected probabilities are shown on a log scale to improve visualization of data below 10%.

Our micropipette assay estimates the adhesion probability P from repeated tests of individual cell pairs. The site densities, m_r and m_ℓ, of the receptors and ligands may be broadly distributed in cell populations. However, only the population means, not the variances, are accounted for in the models (Eqs. 2 and 3). Therefore, it seems reasonable to assume that the variance of P, σ_P^2, is primarily due to the cell-to-cell variations in m_r and m_ℓ. Because m_r and m_ℓ are being considered here as random variables, it follows that the product $m_r m_\ell$ is also a random variable. It can be estimated from Eq. 2 that

$$\sigma_P^2 \approx \sigma_{m_r m_\ell}^2 \left[\frac{\partial P}{\partial (m_r m_\ell)}\right]^2 = \sigma_{m_{rl}}^2 \left[\frac{(1-P)\ln(1-P)}{m_r m_\ell}\right]^2 .$$

Further assuming that the standard deviation of $m_r m_\ell$, $\sigma_{m_r m_\ell}$, is proportional to the mean (constant coefficient of variation), a model for σ_P^2 is generated,

$$\hat{\sigma}_P^2 = \delta^2[(1-P)\ln(1-P)]^2 ,$$

where δ is the coefficient of variation for $m_r m_\ell$. ($\hat{}$ represents an estimator of the quantity under the caret.) This function has a maximum at $P = 0.63$, but diminishes to zero as $P \to 0$. There is in practice, however, a nonzero minimum variance that incorporates other less significant variance sources. For example, we estimate P from a hundred observations; hence P has a resolution no better than 0.5%. To accommodate these other sources, we include an additional constant term, δ_o, so the model becomes

$$\hat{\sigma}_P^2 = \delta_o^2 + \delta^2[(1-P)\ln(1-P)]^2 . \qquad \text{(A2)}$$

Estimates for the two variance parameters, δ_o and δ, can be found by ordinary nonlinear regression of Eq. A2 to the squared residuals. However, to minimize the influence of outliers, it was found to be more appropriate to fit the square root of the variance model (the standard deviation model) to the absolute value of the residuals (Fig. 5).

Because, with this approach, the estimated variances (and therefore the weights) depend on the expected response P itself, the solution to the problem becomes an iterative one. First, an initial estimate for $\mathbf{b}$ (i.e., kinetic rate and binding affinity constants) was found by unweighted (ordinary) least-squares. The estimated responses $\hat{P}_j$ ($= f(\mathbf{x}_j, \hat{\mathbf{b}})$) and the absolute residuals were used to compute the variance parameters δ_o and δ. A set of weights was then derived (from $w_j = c/\hat{\sigma}_P^2(\hat{P}_j)$) and a weighted least-squares regression was performed to estimate a new $\mathbf{b}$. At least three cycles were executed to reach convergence (Carroll and Ruppert, 1988, Chapter 2; Neter et al., 1996, Chapter 10).

The final standard deviation model ($\hat{\sigma}_P$ versus P curve) is shown superimposed over the residuals in Fig. 5. Note that tight variances are expected when adhesion probability is very low or very high, hence the resolution of the assay is maximal with midrange frequency data. A plot of the absolute weighted residuals, $\sqrt{w_j}|\varepsilon_j|$, against the expected response P confirmed the reduction in heteroscedasticity (not shown). For all micropipette data analyzed in this manner, δ ranged between 12 and 16% and δ_o ranged between 0.5 and 2%. The relatively low value for δ indicated acceptable uniformity in the expression level of CD16b on the transfectants and in the IgG coating density on the RBCs.

Normal distribution of residuals

The normality of the distribution of the weighted residuals was verified by ordering the N residuals from low to high, computing the expected normal value for the jth residual, and plotting the results against the actual residuals (a normal probability plot, not shown). The linear diagonal pattern indicated that the residuals were approximately normally distributed and so the requirements of least-squares regression were met without further adjustments (Neter et al., 1996, Chapter 3).

Nonlinear prediction intervals on the mean

Once an iteratively reweighted, nonlinear least-squares problem converges, we have estimates for the M-dimensional vector of regression parameters $\mathbf{b} = \hat{\mathbf{b}}$ and can compute the $M \times M$ asymptotic covariance matrix $\mathbf{\Lambda}$ from

$$\mathbf{\Lambda} = c\left[\frac{df_j^T}{d\mathbf{b}}\,\mathbf{W}\frac{df_j}{d\mathbf{b}}\right]^{-1}\Bigg|_{\hat{\mathbf{b}}},$$

where $df_j/d\mathbf{b}$ is an $N \times M$ matrix of derivatives of the model function $y_j = f(\mathbf{x}_j, \mathbf{b})$ (the single-species model, Eq. 2), with the jth row evaluated at $\mathbf{x}_j$. $\mathbf{W}$ is an $N \times N$ diagonal matrix of weights w_j, and c is the proportionality constant relating the weights to the true residual variances, as discussed earlier (Jennrich, 1995, Chapter 8; Neter et al., 1996, Chapter 10).

The resulting fit parameters and their covariance matrices can be used to establish prediction intervals for the mean response to mixed-isotype conditions. Let $g(\mathbf{z}, \mathbf{b})$ be a nonlinear function of the fit parameters $\mathbf{b}$ and predictor variables $\mathbf{z}$. Here g is the dual-species concurrent binding model (Eq. 3). We wish to predict the mean response g and the confidence interval for the mean response at $\mathbf{z} = \mathbf{z}_o$ from a predetermined $\hat{\mathbf{b}}$ with covariance $\mathbf{\Lambda}$. (This is more restrictive than the confidence interval on the response, which would describe the distribution of all responses at $\mathbf{z} = \mathbf{z}_o$.) This is usually referred to as a prediction interval on the mean, and is given by (Carroll and Ruppert, 1988, Chapter 2; Jennrich, 1995, Chapter 8)

$$\text{mean response} \pm (1-\alpha)\%\ \text{confidence interval}$$
$$= g(\mathbf{z}_o, \hat{\mathbf{b}}) \pm t_{N-M}^{1-\alpha/2} \times \sqrt{\frac{dg}{d\mathbf{b}}\,\mathbf{\Lambda}\,\frac{dg^T}{d\mathbf{b}}\Bigg|_{\mathbf{z}_o,\hat{\mathbf{b}}}}, \qquad \text{(A3)}$$

where α is chosen to be 0.05 for prediction intervals with 95% confidence levels. Here g is different from the single-species model f (Eq. 2) used to generate $\mathbf{b}_i$ and $\mathbf{\Lambda}_i$ for each single species. The five-dimensional vector $\mathbf{z}$ ($= \{m_{r_1}, m_{\ell_1}, m_{r_2}, m_{\ell_2}, t\}^T$) is evaluated at $\mathbf{z}_o$, which generally takes component values different from those of the two 3D predictor variable vectors, $\mathbf{x}_i = \{m_{r_i}, m_{\ell_i}, t\}^T$ ($i = 1, 2$). The vector $dg/d\mathbf{b}$ is developed from the four-dimensional fit-parameter vector $\mathbf{b}$ ($= [\mathbf{b}_1^T, \mathbf{b}_2^T]^T = \{A_c K_{a1}, k_{r1}, A_c K_{a2}, k_{r2}\}^T$) and is then evaluated at $\mathbf{b} = \hat{\mathbf{b}}$, the component values of which have previously been determined from the two single-isotype regressions. The 4×4 covariance matrix $\mathbf{\Lambda}$ is similarly constructed from the two single-isotype 2×2 covariance matrices, $\mathbf{\Lambda}_1$ and $\mathbf{\Lambda}_2$, according to

$$\mathbf{\Lambda} = \begin{bmatrix} \mathbf{\Lambda}_1 & \mathbf{0} \\ \mathbf{0} & \Lambda_2 \end{bmatrix}.$$

Thus, the location of the mean response and the width of the its confidence interval (Eq. A3) for a given dual-species condition $\mathbf{z}_o$ are determined by the fitted single-species binding parameters and their variability, estimated a priori from completely independent experiments and model functions.

We would like to thank Dr. S. Nagarajan for invaluable technical assistance. We also thank Dr. Ping Li for iodination of the CLBFcgran1 Fab mAb. This work was supported by National Science Foundation grants BCS 9210648 and BCS 9350370 and National Institutes of Health (NIH) grant AI38282 (CZ) as well as NIH grant AI30631 (PS). TEW was also partially supported by NIH Training Grant GM08433.

REFERENCES

Bell, G. I. 1978. Models for the specific adhesion of cells to cells. *Science.* 200:618–627.

Bell, G. I., M. Dembo, and P. Bongrand. 1984. Cell adhesion: competition between nonspecific repulsion and specific bonding. *Biophys. J.* 45: 1051–1064.

Bikoue, A., F. George, P. Poncelet, M. Mutin, G. Janossy, and J. Sampol. 1996. Quantitative analysis of leukocyte membrane antigen expression: normal adult values. *Cytometry.* 26:137–147.

Burton, D. R. 1985. Immunoglobulin G: functional sites. *Mol. Immunol.* 22:161–206.

Carroll, R. J., and D. Ruppert. 1988. Transformation and Weighting in Regression. Chapman and Hall, New York.

Chesla, S. E., P. Li, S. Nagarajan, P. Selvaraj, and C. Zhu. 2000. The membrane anchor influences ligand binding 2D kinetic rates and 3D affinity of FcγRIII (CD16). *J. Biol. Chem.* 275:10235–10246.

Chesla, S. E., P. Selvaraj, and C. Zhu. 1998. Measuring two-dimensional receptor-ligand binding kinetics by micropipette. *Biophys. J.* 75: 1553–1572.

Clark, M. R., S. G. Stuart, R. P. Kimberly, P. A. Ory, and I. M. Goldstein. 1991. A single amino acid distinguishes the high-responder from the low-responder form of Fc receptor II on human monocytes. *Eur. J. Immunol.* 21:1911–1916.

Clynes, R., Y. Takechi, Y. Moroi, A. Houghton, and J. V. Ravetch. 1998. Fc receptors are required in passive and active immunity to melanoma. *Proc. Natl. Acad. Sci. USA.* 95:652–656.

Dumaswala, U. J., M. J. Wilson, T. Jose, and D. L. Daleke. 1996. Glutamine- and phosphate-containing hypotonic storage media better maintain erythrocyte membrane physical properties. *Blood.* 88:697–704.

Dustin, M. L., L. M. Ferguson, P.-Y. Chan, T. A. Springer, and D. E. Golan. 1996. Visualization of CD2 interaction with LFA-3 and determination of the two-dimensional dissociation constant for adhesion receptors in a contact area. *J. Cell. Biol.* 132:465–474.

Fridman, W. H. 1989. Structures and Functions of Low Affinity Fc Receptors. Karger, Basel, New York.

Fridman, W. H. 1997. Structure and function of immunoglobulins. *In* Cell-Mediated Effects of Immunoglobulins. W. H. Fridman and C. Sautes, editors. R. G. Landes, Austin, TX. 1–27.

Huizinga, T. W., M. Kerst, J. H. Nuyens, A. Vlug, A. E. von dem Borne, D. Roos, and P. A. Tetteroo. 1989. Binding characteristics of dimeric IgG subclass complexes to human neutrophils. *J. Immunol.* 142: 2359–2364.

Jefferis, R., and D. S. Kumararatne. 1990. Selective IgG subclass deficiency: quantification and clinical relevance. *Clin. Exp. Immunol.* 81:357–367.

Jennrich, R. I. 1995. An Introduction to Computational Statistics: Regression Analysis. Prentice Hall, Englewood Cliffs, NJ.

Kuo, S. C., and D. A. Lauffenburger. 1993. Relationship between receptor/ligand binding affinity and adhesion strength. *Biophys. J.* 65:2191–2200.

Lauffenburger, D. A., and J. J. Linderman. 1993. Receptors: Models for Binding, Trafficking, and Signaling. Oxford University Press, New York.

Lowry, M. B., A. M. Duchemin, J. M. Robinson, and C. L. Anderson. 1998. Functional separation of pseudopod extension and particle internalization during Fcγ receptor-mediated phagocytosis. *J. Exp. Med.* 187:161–176.

Nagarajan, S., S. Chesla, L. Cobern, P. Anderson, C. Zhu, and P. Selvaraj. 1995. Ligand binding and phagocytosis by CD16 (Fcγ receptor III) isoforms. Phagocytic signaling by associated ζ and γ subunits in Chinese hamster ovary cells. *J. Biol. Chem.* 270:25762–25770.

Nayve, F. R., Jr., T. Misato, M. Matsumura, and H. Kataoka. 1994. HBs-MAb production in perfusion culture with selective ammonia removal system. *J. Biotechnol.* 34:217–225.

Neter, J., M. H. Kutner, C. J. Nachtsheim, and W. Wasserman. 1996. Applied Linear Statistical Models: Regression, Analysis of Variance, and Experimental Designs. Irwin, Homewood, IL.

Poncelet, P., and P. Carayon. 1985. Cytofluorometric quantification of cell-surface antigens by indirect immunofluorescence using monoclonal antibodies. *J. Immunol. Methods.* 85:65–74.

Powell, M. S., M. D. Hulett, R. I. Brinkworth, and P. M. Hogarth. 1996. Human FcγR: Ligand interactions. *In* Human IgG Fc Receptors. J. G. J. van de Winkel and P. J. A. Capel, editors. R. G. Landes, Austin, TX. 5–23.

Rascu, A., R. Repp, N. A. C. Westerdaal, J. R. Kalden, and J. G. J. van de Winkel. 1997. Clinical relevance of Fcγ receptor polymorphisms. *Ann. NY Acad. Sci.* 815:282–295.

Reuveny, S., D. Velez, J. D. Macmillan, and L. Miller. 1986. Factors affecting cell growth and monoclonal antibody production in stirred reactors. *J. Immunol. Methods.* 86:53–59.

Salmon, J. E., J. C. Edberg, and R. P. Kimberly. 1996. FcγR on neutrophils. *In* Human IgG Fc Receptors. J. G. J. van de Winkel and P. J. A. Capel, editors. R. G. Landes, Austin, TX. 79–105.

Sautes, C. 1997. Structure and expression of Fc receptors (FcR). *In* Cell-Mediated Effects of Immunoglobulins. W. H. Fridman and C. Sautes, editors. R. G. Landes, Austin, TX. 29–65.

Selvaraj, P., O. Carpen, M. L. Hibbs, and T. A. Springer. 1989. Natural killer cell and granulocyte Fcγ receptor III (CD16) differ in membrane anchor and signal transduction. *J. Immunol.* 143:3283–3288.

Selvaraj, P., M. L. Dustin, R. Mitnacht, T. Hunig, T. A. Springer, and M. L. Plunkett. 1987. Rosetting of human T lymphocytes with sheep and human erythrocytes. Comparison of human and sheep ligand binding using purified E receptor. *J. Immunol.* 139:2690–2695.

Selvaraj, P., W. F. Rosse, R. Silber, and T. A. Springer. 1988. The major Fc receptor in blood has a phosphatidylinositol anchor and is deficient in paroxysmal nocturnal haemoglobinuria. *Nature.* 333:565–567.

Serke, S., A. van Lessen, and D. Huhn. 1998. Quantitative fluorescence flow cytometry: a comparison of the three techniques for direct and indirect immunofluorescence. *Cytometry.* 33:179–187.

Warmerdam, P. A., J. G. van de Winkel, E. J. Gosselin, and P. J. Capel. 1990. Molecular basis for a polymorphism of human Fcγ receptor II (CD32). *J. Exp. Med.* 172:19–25.

Williams, T. E. 1998. Adhesion of membrane-bound receptors and ligands: Concurrent binding and the role of microtopology. Ph.D. thesis. Georgia Institute of Technology, Atlanta.

Williams, T. E., S. Nagarajan, P. Selvaraj, and C. Zhu. 2000. Concurrent and independent binding of Fcγ receptors IIa and IIIb to surface-bound IgG. *Biophys. J.* 79:1867–1875.

Wolfram Research. 1996. Mathematica 3.0 Standard Add-on Packages. Wolfram Media and Cambridge University Press, New York.

Zhu, C., and T. E. Williams. 2000. Modeling concurrent binding of multiple molecular species in cell adhesion. *Biophys. J.* 79:1850–1857.